Tellus (2004), 56B, 72–84
Printed in UK. All rights reserved

TELLUS

The dynamics of the North Atlantic carbon cycle and its relation to the temperature of the winter mixed layer

By GÖRAN BROSTRÖM*, *Göteborg University, Earth Science Centre, Department of Oceanography, Box 460, S-405 30 Göteborg, Sweden*

(Manuscript received 22 May 2002; in final form 7 July 2003)

ABSTRACT

Property–property relationships between oceanic carbon species and physical parameters have been used extensively to extrapolate sparse measurements to larger areas. However, the physical processes behind the applied relationships are not always described, implying that uncertainties are introduced to the method. In this study, it is shown that the dynamical features of the North Atlantic carbon cycle can be condensed into a simple framework by focusing on the properties of the winter mixed layer and the equilibrium concentration of the system. The change in the equilibrium concentration between the Sargasso Sea and the Nordic seas is about 250 μmol kg^{-1}, where 50 μmol kg^{-1} is due to the corrections from the annual cycles in sea surface temperature and biological production. A theoretical framework that focuses on the relation between variables and the temperature of the winter mixed layer is presented and analyzed in some detail using results from a general circulation model. The derived model predicts that there is a tight relation between the total dissolved inorganic carbon concentration and the temperature in the winter mixed layer, and such relation can indeed be found from the TTO/NAS expedition data. Furthermore, the analysis shows that the system is relatively close to the equilibrium concentration in the Sargasso Sea but that the system is highly undersaturated in the Nordic seas. Further, the analysis shows that both the entrainment of carbon-rich deep water and the air–sea flux of CO_2 must be correctly accounted for to describe the system.

1. Introduction

Without doubt temperature has a strong impact on the oceanic carbon system. Either direct through the solubility of the dissolved inorganic carbon or through dynamical reasons such as its importance for mixing, etc. Thus, in many regions of the world there exists a clear relation between properties of the carbon system and the oceanic temperature (Broecker and Peng, 1982; Chen et al. 1990; Takahashi et al. 1993; Broström, 1997). These simple relationships—and other property–property plots for various chemical species—are helpful for understanding the basic structure and dynamics of the oceanic carbon system. Thus, these kinds of graphs represent a way to make the most of the sparse and hard won measurements on the carbon species.

In addition to being valuable in itself, relations between, for example, the partial pressure of CO_2 in the surface water (pCO_2), and the temperature is useful for mapping pCO_2 on to the well-known temperature field. This method of extrapolating pCO_2 measurements to large areas is widespread and has had a major impact on our present view of the carbon system (Tans et al. 1990; Watson et al. 1991; Stephens et al. 1995; Lee et al. 1998; Sabine and Key, 1998; Feely et al. 1999; Loukos et al. 2000). An obvious difficulty with the method is that a unique relationship between the interpolated variable and the temperature must be applied for each region. Also, there may be different relationships during different seasons.

Although the presumed relation between pCO_2 and the temperature has been used extensively in the interpolation/mapping procedure, the underlying dynamics of the relationships have not received much attention (Sabine and Key, 1998; Lefèvere and Taylor, 2002). For instance, although the temperature dependent carbon solubility is important for the large-scale distribution of carbon, deviations from equilibrium are not set by the solubility itself. Rather, other processes such as surface heat flux, upwelling, biological production, etc. are important for the magnitude of the disequilibrium (Peng et al. 1987; Takahashi et al. 1993; Sarmiento et al. 1995; Follows et al. 1996; Cooper et al. 1998; Murnane et al. 1999; Broström, 2000; Lefèvere and Taylor, 2002). These processes are not necessarily directly linked to the temperature itself. Thus, more sophisticated approaches are needed to outline and understand the basic features of the observed property–property relationships used for extrapolating the carbon system properties (Sabine and Key, 1998; Lefèvere and Taylor, 2002).

*Present address: Department of Meteorology, Stockholm University, S-106 91 Stockholm, Sweden.
e-mail: goran@misu.su.se

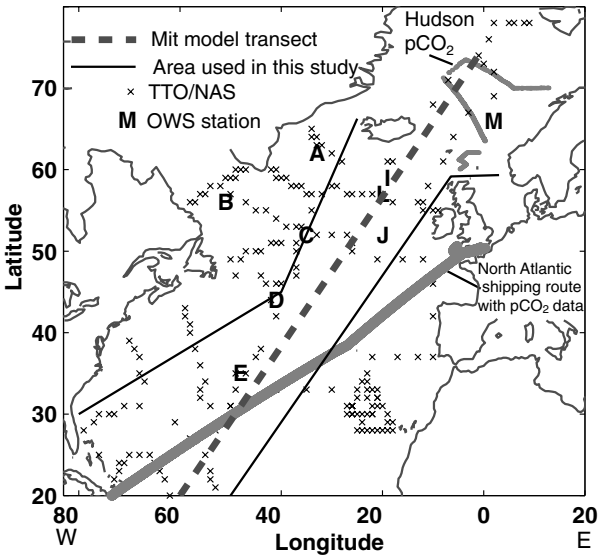

Fig 1. An outline of the area focused on in this study. The positions of data used in the study are also displayed. The data are from the Ocean Weather Stations, the TTO/NAS expedition in 1981 (Brewer et al. 1986), underway pCO_2 data from the Hudson cruise in 1982 (Weiss et al. 1992), and underway pCO_2 data from a North Atlantic shipping route (from February 1995; Cooper et al. 1998).

In this study, the dynamics of the carbon cycle in the "Gulf-Stream" part of the North Atlantic (Fig. 1) is investigated. Although earlier studies could not prove a simple relation between carbon species and temperature in the TTO/NAS dataset (Broecker et al. 1985; Brewer et al. 1986) it is shown that such relationships can be found by focusing on the winter mixed layer. Here, the observed relationship is analyzed in some detail by focusing on the state that is in equilibrium with the atmosphere, and the dynamics that forces the system away from equilibrium. Following (Broström, 1997, 2000), the annually averaged air–sea flux of CO_2, $\overline{F_{C_T}}$, can be expressed as

$$\overline{F_{C_T}} = \alpha \left(C_T^W - C_{eq} \right), \tag{1}$$

where C_T^W is the C_T concentration in the winter mixed layer, α (m yr^{-1}) is a rate constant, C_{eq} is the dynamical equilibrium concentration and is defined as the C_T concentration of the winter mixed layer that would give zero flux of CO_2 over one annual cycle.

The dynamical equilibrium concentration reflects the annual average of several processes, hence

$$C_{eq} = C_{eq}^W + \Delta C_{eq}^{SST} + \Delta C_{eq}^B \tag{2}$$

where C_{eq}^W is defined as the C_T concentration that is in equilibrium with the atmospheric pCO_2: ΔC_{eq}^{SST} reflects the influence of the annual sea surface temperature (SST) cycle on the equilibrium concentration and ΔC_{eq}^B is the correction due to biological production (see also Broström, 2000).

A simple model is developed for the area under consideration; model results and data indicate that the water is slightly undersaturated, say less then 10–20 μmol kg^{-1} undersaturation, in the main part of the northern North Atlantic. This is the result of relatively weak heat flux in this part of the North Atlantic, but also because of large entrainment of carbon-rich deep waters that reduces the undersaturation. In fact, for the main part of the North Atlantic, the entrainment dominates over the air–sea flux of CO_2 as the factor that keeps the system close to saturation. In the Nordic seas there is a net export of carbon from the upper ocean; furthermore, there is a strong heat fluxes in this area and the system is about 50 μmol kg^{-1} below saturation in the northwestern Nordic seas. According to this study, the observed undersaturations are due to several interacting mechanisms, and no simple explanation can be given.

The theoretical concepts needed for this study are presented in Section 2. The diagnostic quantities defined in Section 2 are quantified in Section 3 using the MIT biogeochemical ocean model. A simple model that describes the basic features of the carbon cycle in the "poleward-moving" water of the North Atlantic is described in Section 4. Section 5 is devoted to discussions.

2. Some theoretical concepts

2.1. Basic considerations

Let us consider the system outlined in Fig. 2; that is, a quantity C^W that changes along a Lagrangian coordinate ξ subject to horizontal fluxes Q_C, fluxes through the sea surface, $-F_C$, fluxes through the permanent thermocline M_C, and export by particles through the main thermocline, B_C. Since the seasonal thermocline is an important factor for the carbon cycle changes over a certain distance $\Delta\xi$ corresponding to the distance (or time) between two situations that correspond to the winter mixed layer will be considered (Fig. 2). Accordingly,

$$\frac{Q_C(\xi_0 + \Delta\xi) - Q_C(\xi_0)}{\Delta\xi} = -\overline{F_C} + \overline{M_C} - \overline{B_C}, \tag{3}$$

where

$$\overline{F_C} = \frac{1}{\Delta\xi} \int_{\xi}^{\xi+\Delta\xi} F_C(\xi)\, d\xi,$$

$$\overline{M_C} = \frac{1}{\Delta\xi} \int_{\xi}^{\xi+\Delta\xi} M_C(\xi)\, d\xi, \tag{4a–c}$$

$$\overline{B_C} = \frac{1}{\Delta\xi} \int_{\xi}^{\xi+\Delta\xi} B_C(\xi)\, d\xi.$$

For mathematical reasons it is useful to rewrite eq. (3) as a differential such that

$$\frac{dQ_C}{d\xi} = -\overline{F_C} + \overline{M_C} - \overline{B_C}. \tag{5}$$

The dynamical features behind the horizontal flux of heat, total inorganic carbonate and nitrate concentrations are to a large

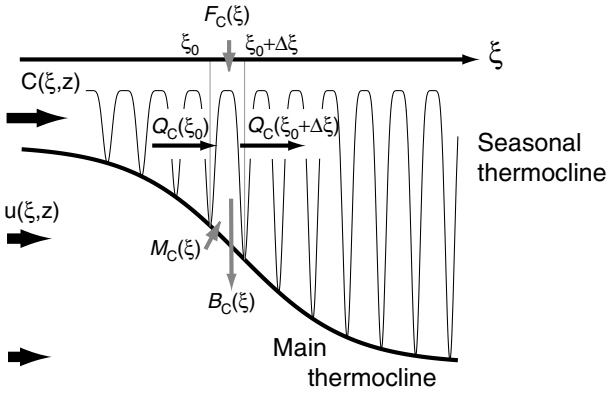

Fig 2. Schematic sketch for the fluxes described in Section 2. The model is based on the assumption that there exist a coordinate ξ that follow a water column moving with the northward drift in the North Atlantic. The column is subject to an annual cycle in mixing, and a changing large-scale structure of the main thermocline. Taking a control volume corresponding to the distance between two events where the mixing reaches to the main thermocline it follows that fluxes through the control surfaces are: horizontal fluxes $Q_C(\xi)$ and $Q_C(\xi + \Delta\xi)$, air–sea flux F_C, advective and diffusive fluxes through the bottom surface M_C, finally, there may also be a particle induced flux of C through the bottom boundary, B_C.

extent similar; thus, it is likely that the transport of a concentration C can be described by the flux of temperature times the gradient of the concentration with respect to the temperature (Walin, 1977). Based on this assumption, let us assume *a priori* that eq. (5) can be written as (see also Appendix A)

$$\frac{dQ_T}{d\xi}\frac{dC^W}{dT^W} = -\overline{F_C} + \overline{M_C} - \overline{B_C}, \tag{6}$$

where Q_T is the horizontal flux of heat and dC^W/dT^W is the horizontal relation between C^W and T^W (note that C^W and T^W refer to the values of the winter mixed layer).

If eq. (6) is applied to temperature then $\overline{B_T}$ is zero; furthermore, a reasonable assumption for the North Atlantic is $\overline{F_T} \gg \overline{M_T}$ such that

$$\frac{dQ_T}{d\xi} = -\overline{F_T}. \tag{7}$$

For nitrogen, the air–sea flux of nutrients is negligible and

$$\frac{dQ_T}{d\xi}\frac{d\mathrm{NO}_3^W}{dT^W} = \overline{M_{\mathrm{NO}_3}} - \overline{B_{\mathrm{NO}_3}}. \tag{8}$$

For total inorganic carbonate all fluxes are important, thus

$$\frac{dQ_T}{d\xi}\frac{dC_T^W}{dT^W} = -\overline{F_{C_T}} + \overline{M_{C_T}} - \overline{B_{C_T}}. \tag{9}$$

The biological tissues follow the Redfield ratio $\gamma_{C:N}$; thus $\overline{B_{C_T}} = \gamma_{C:N}\overline{B_{\mathrm{NO}_3}}$. Furthermore, the transport through the main thermocline in the North Atlantic is to a large extent forced by the biological cycle such that $\overline{M_{C_T}} \approx \gamma_{C:N}\overline{M_{\mathrm{NO}_3}}$. It should be noted that there is also a vertical flow induced by the solubility pump, $\overline{m_S}$, and the invasion of anthropogenic carbon into the ocean, $\overline{m_A}$; however, as will be shown in the next section these are small compared with $\overline{F_{C_T}}$ and will be neglected in this framework. Using $\overline{M_{C_T}} - \overline{B_{C_T}} \approx \gamma_{C:N}(\overline{M_{\mathrm{NO}_3}} - \overline{B_{\mathrm{NO}_3}}) = \gamma_{C:N} d\mathrm{NO}_3^W/d\xi$, and applying eq. (7) it follows that

$$\frac{dC_T^W}{dT^W} - \gamma_{C:N}\frac{d\mathrm{NO}_3^W}{dT^W} = \frac{\overline{F_{C_T}}}{F_T}. \tag{10}$$

The approximate relation put forward in eq. (10) is useful for interpreting and evaluating the distribution of C_T^W if there is a clear relation between C_T^W and T^W. The relation may also be used to design accurate interpolation schemes for mapping properties of the carbon system onto temperature.

3. Results from a general circulation model

In this section, some results from a general circulation model (GCM) will be presented to verify: (1) that the C:N ratio of entrained water is approximately similar to the C:N ratio of the biological production; (2) that the model outlined in Section 2 describes all the main flows of the carbon system. Furthermore, the parameters α and C_{eq} (and parameters involved in C_{eq}) in eqs. (1) and (2) will be evaluated.

3.1. *Outline of the model*

The MIT ocean model is built around a finite-difference representation of the hydro-dynamical equations that describe the basic features of the ocean (Marshall et al. 1997a,b). The model uses a constant turbulent exchange coefficient to mimic the small-scale turbulence and an eddy transfer scheme to describe the large-scale lateral mixing (Gent et al. 1995).

The biogeochemical model runs in an off-line mode where nitrate and total dissolved inorganic carbon concentrations are the prognostic variables (Follows et al. 1996). The forcing fields are updated monthly, and the model reproduces the annual cycles in temperature and vertical mixing. To simulate the biological export of nutrients and carbon, the model includes a light-dependent removal rate for the upper ocean that accounts for the most prominent features of the upper-ocean nutrient cycles. The model experiments are carried out either with an atmospheric $p\mathrm{CO}_2$ that reproduces the changes between 1880 to 1981 (starting from the steady state for 1880) or with a constant $p\mathrm{CO}_2$ depending on the aim of the experiments.

In this study the carbon to nitrogen ratio is taken to be $\gamma_{C:N} = 9$; this is somewhat higher than the Redfield ratio, $\gamma_{C:N} = 106{:}16$, but is appropriate for the northern North Atlantic (Sambrotto et al. 1993; Broström, 1998; Daly et al. 1999; Broström, 2000; Körtzinger et al. 2001). Processes such as nitrogen fixation and production of calcium carbonate can significantly alter $\gamma_{C:N}$. The C:N ratio used in this study should be viewed as a large-scale estimate of all these processes.

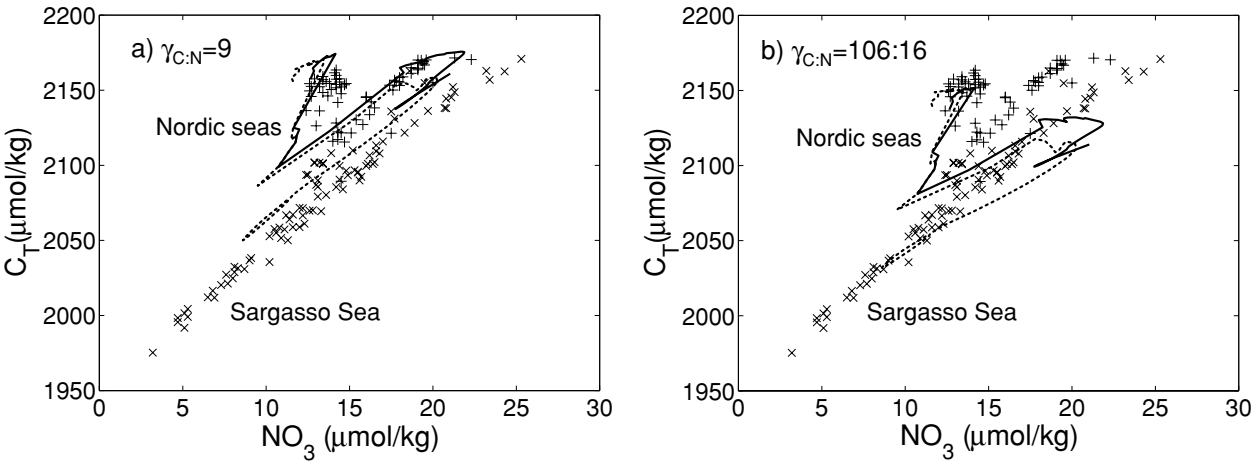

Fig 3. Data and model results from the thermocline: (a) model results with $\gamma_{C:N} = 9$ and (b) model results for $\gamma_{C:N} = 106{:}16$. Data are from the TTO/NAS dataset (Brewer et al. 1986) and represent measurements between 500–700 m for the selected area; data with temperatures above 7 °C are marked as (×) and below 7 °C as (+). The model predictions are taken along the transect defined in Fig. 1 and the lines corresponds to the depth intervals 360–510 m (dashed line) and 510–710 m (full line). Data for temperatures above 7 °C (the Sargasso Sea) are close to a straight line with a slope of $\Delta C{:}\Delta N = 9$. The C_T is shown as normalized to 35 psu.

3.2. The C:N ratio of entrained water

Entrainment of thermocline water that is rich in nitrogen and carbon is important for the poleward-moving water in the North Atlantic. For the area defined in Fig. 1, the thermocline is presumably located between 500–700 meters, and data from this area and depth interval are shown in Fig. 3. The results from the MIT biogeochemical model are taken from the experiments with a realistic evolution of the atmospheric pCO_2. Two experiments with different C:N ratios for biological production are shown in the figures: Fig. 3a reflects an experiment with $\gamma_{C:N} = 9$ and Fig. 3b reflects an experiment with $\gamma_{C:N} = 106{:}16$.

The model gives reasonable results on the C_T concentration at 500–700 m depth for $\gamma_{C:N} = 9$ (Fig. 3a), although somewhat high C_T concentrations are produced in the model. The experiments show that the signal in the thermocline to a large extent reflects the C:N ratio of biological production. The data from the Sargasso Sea display a relation that is close to linear with a $\Delta C{:}\Delta N$ ratio of 9; the experiment with $\gamma_{C:N} = 9$ is closest to these data, showing that $\gamma_{C:N} = 9$ is consistent with thermocline data of the North Atlantic (note that the model describe the anthropogenic pCO_2 signal in both experiments).

3.3. Estimating the strength of flows

It is not straightforward to diagnose the fluxes in eq. (14) along a line in the North Atlantic and describe its relation to the temperature. To find the strength of the various fluxes, the change in C_T that the modeled fluxes would give rise to over one yr is taken as a measure of their strengths. This is achieved using the fluxes from the C_T field to force a new field with the same physical forcing as the original field. The concentration of the winter mixed layer in the following year is taken as a measure of the strength of each process. Although this does not represent a true diagnostic value of the fluxes, it should provide a reasonable estimate on their relative strengths.

These experiments use $\gamma_{C:N} = 9$, a realistic time evolution of pCO_2 in the atmosphere and the fluxes are evaluated for 1981. The nitrate field is in steady state, implying that the transport of NO_3 is exactly canceled out by the biological production. Thus, in the following discussion the influence of the biological cycle is subtracted by removing the transport of $\gamma_{C:N}\,NO_3$, which may be viewed as the biological forcing on the carbon system. The following fluxes are displayed in Fig. 4: the strength of the air–sea flux of CO_2 (i.e. $\overline{F_{C_T}}$); the strength of the advection and diffusion of $C_T - \gamma_{C:N}NO_3$ (the advection–diffusion of the "non-nitrogen" or "non-biological" part of the carbon cycle); finally, $\overline{m_S} + \overline{m_A}$ and $\overline{m_S}$ are also shown. The quantity $\overline{m_S} + \overline{m_A}$ is calculated from the full fluxes of the model, subtracting the influence from the air–sea flux and the advection diffusion of $C_T - \gamma_{C:N}NO_3$. The strength of $\overline{m_S}$ is evaluated from a similar set of experiments performed for a steady-state run with pCO_2 = 278 ppm in the atmosphere (representing the year 1880).

Figure 4 shows that the quantity $\overline{m_S} + \overline{m_A}$ is small compared with the strength of the air–sea flux of CO_2 for the selected transect. Furthermore, the experiment shows that the actual increase in concentration due to time evolution in the atmospheric pCO_2 is small. The conclusion is that the CO_2 from the air–sea flux is transported horizontally in the model rather than being mixed downward into the thermocline. This is consistent with observations that there are strong horizontal currents in the northern North Atlantic in combination with strong horizontal gradients in C_T. The basic *a priori* assumptions of the simple model in Section 2 are thus verified.

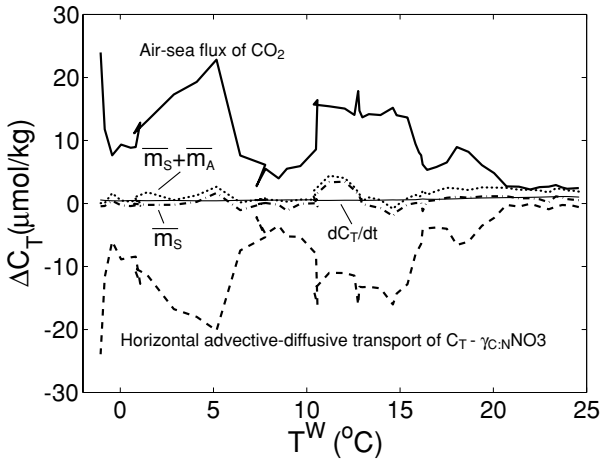

Fig 4. The strength of the fluxes in the MIT biogeochemical model. The figure show the increase in concentration that each term should give rise to after one year of integration (corresponding to year 1981). Shown are the following: the air–sea flux of CO_2; the horizontal advective–diffusive transport of the "non-nitrogen part" of C_T; the vertical transports $\overline{m_S}$ and $\overline{m_A}$; and the net increase in C_T over the year (the system evolves as a result of the increasing pCO_2 in the atmosphere).

3.4. *The dynamical equilibrium concentration*

In Broström (2000) the quantities α, ΔC_{eq}^{SST} and ΔC_{eq}^{B} were estimated for the Ocean Weather Stations (OWS) in the North Atlantic using a combination of data and results from a one-dimensional model. Here some of these results will be used for two independent estimates on the parameters. The positions of the OWS stations used in this study are shown in Fig. 1, and some results from these stations are displayed in Fig. 5 together with results from the MIT biogeochemical model.

3.4.1. Model predictions on α, C_{eq}^{W}, ΔC_{eq}^{SST} and ΔC_{eq}^{B}. The dynamical equilibrium concentration is defined as the concentration that the winter mixed layer takes in the absence of advection. Accordingly, the advection is turned off in the model and the integration is continued until there is a repeating cycle in C_T. The model thus reaches a state where the annual cycle is in equilibrium with the prevailing atmospheric partial pressure of CO_2, which is taken to be 340 ppm in these experiments. The model predictions on C_T in the winter mixed layer can thus be interpreted in terms of the dynamical equilibrium concentration for C_T^W. There are three parameters, C_{eq}^{W}, ΔC_{eq}^{SST} and ΔC_{eq}^{B}, that are important for the dynamical equilibrium concentration and three distinct model experiments are used to evaluate these parameters.

C_{eq}^{W} is determined by an experiment that does not include the annual cycles in sea surface temperature and biological production. The value of $C_{eq}^{W} + \Delta C_{eq}^{SST}$ is determined by an experiment that includes the annual cycle in sea surface temperature but neglects the biological cycles. The final experiment includes the annual cycles in sea surface temperature and biological production, which gives $C_{eq}^{W} + \Delta C_{eq}^{SST} + \Delta C_{eq}^{B}$. The output from these experiments can be used to estimate C_{eq}^{W}, ΔC_{eq}^{SST} and ΔC_{eq}^{B}; the results from the calculations are displayed in Figs. 5b and c.

The rate at which the system is able to approach equilibrium, α, depends mainly on the wind speed, the sea surface temperature, and the form of the upper ocean mixing cycle (Broström, 2000). Because of the complexity of α, it is not easy to determine its value by a single experiment. However, if $\overline{F_{C_T}}$, C_T^W and C_{eq} are known, then α can be calculated from eq. (1). To find $\overline{F_{C_T}}$ and C_T^W, advection is included and the model is integrated until a repeating cycle is obtained. Given that C_{eq} is calculated in the earlier experiments, α can be calculated and the results are displayed in Fig. 5a.

3.4.2. Some discussion on the model predictions on α, C_{eq}^{W}, ΔC_{eq}^{SST} and ΔC_{eq}^{B}. The rate at which the system is able to approach equilibrium depends on a number of processes. Let us therefore recapitulate some of the results from Broström (2000) using station C as an example: α is related to the annual mean value of the gas exchange coefficient (m yr^{-1}) times the solubility for CO_2 (μmolC kg^{-1} ppm^{-1}); the magnitude of this quantity is about 115 m yr^{-1} μmolC kg^{-1} ppm^{-1}. Furthermore, α depends on the response of pCO_2 to changes in C_T; this dependence can be estimated from a Taylor expansion, and the first-order term has a magnitude of about 2.1 ppm/(μmol C kg^{-1}). Finally, the structure of the annual mixing cycle is important for the effective rate at which the system is able to approach equilibrium. During periods with a shallow mixed layer, the air–sea gas exchange is trapped within the surface layer (Broström, 2000; Lefèvere and Taylor, 2002). The carbon system thus comes relatively close to equilibrium with the atmosphere during this period hampering the equilibration rate of the system (Broström, 2000). There are shallow mixing conditions under a significant part of the annual cycle that reduce the effectiveness of the rate constant α with about 50% at station C (Broström, 2000). Thus, the magnitude of α is about 120 m yr^{-1} as shown in Fig. 5a. The MIT biogeochemical model predicts that α is stronger in the Nordic seas than in the Sargasso Sea. The wind speeds, as well as the sensitivity of the oceanic pCO_2 to changes in C_T, are stronger in the Nordic seas than in the Sargasso Sea.

The influence of the biological production cycle reflects the mean of the annual biological cycle in C_T, weighted with the wind speed. It is represented by ΔC_{eq}^{B}, and it follows the nutrient concentration to a first-order approximation. It is accordingly high in the nutrient-rich Nordic seas, where $\Delta C_{eq}^{B} \approx 20$–$30$ μmol kg^{-1} (the signal for the biological cycle is about 100 μmol kg^{-1} and it lasts for about 0.3 yr), and it is close to zero in the Sargasso Sea. Taking into account that the water temperature in the MIT model is slightly too cold (about 2–3 °C too cold at station M) there is a good agreement between the estimates for the OWS stations and the results from the MIT ocean model on ΔC_{eq}^{B}.

ΔC_{eq}^{SST} represents the annually integrated effect of the sea surface temperature cycle. Results from the MIT biogeochemical

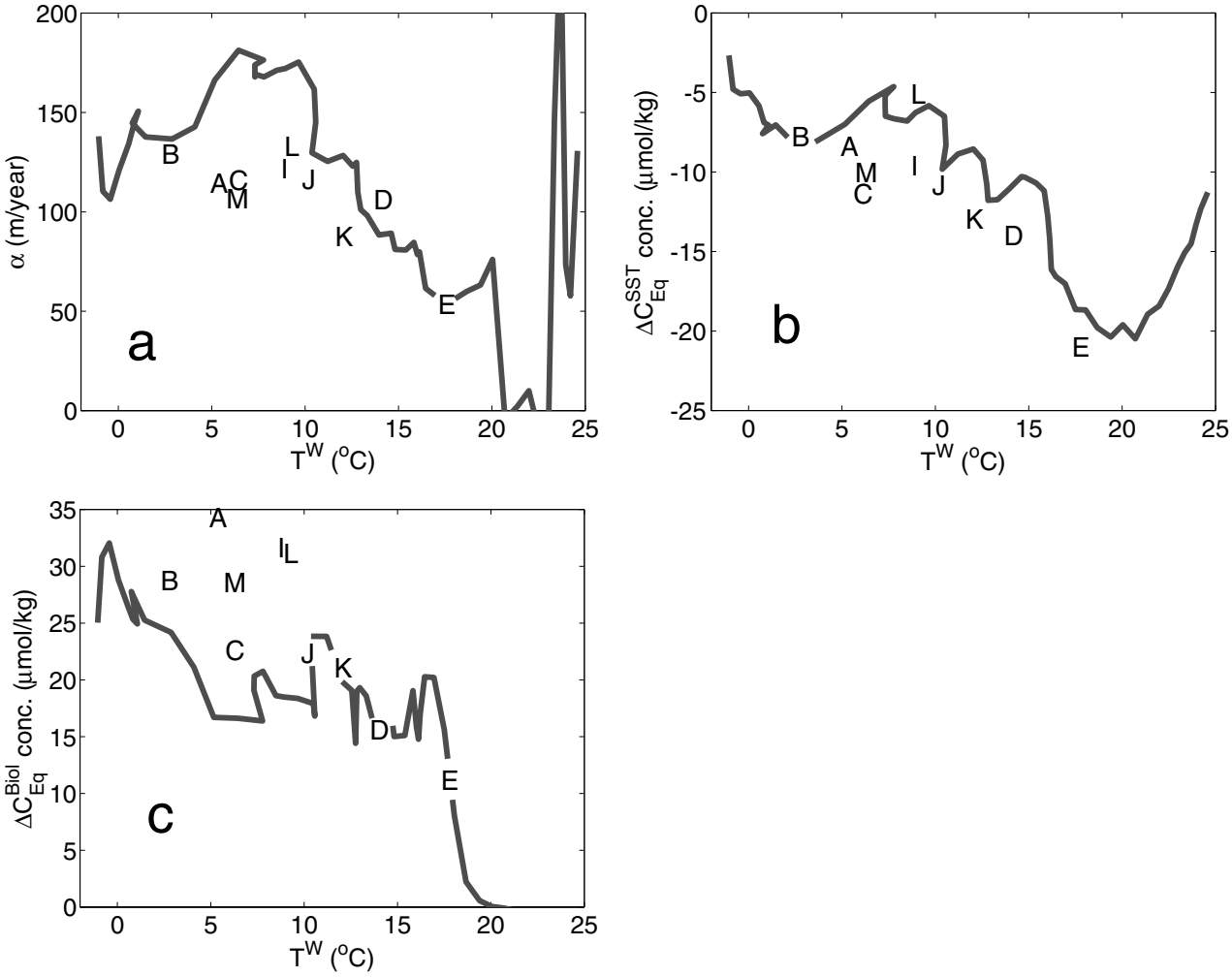

Fig 5. Estimates on α, C_{eq}^{SST} and C_{eq}^{B}, presented in panels a–c, respectively. The solid shows model results from the line defined in Fig. 1; letters represent estimates from some ocean weather stations in the North Atlantic. These data are from Broström (2000).

model show that ΔC_{eq}^{SST} is strongest in the Sargasso Sea with values of -20 μmol kg^{-1}, and it is about -5 μmol kg^{-1} in the northern Nordic seas. The strong variation in ΔC_{eq}^{SST} is due to the following: (1) the annual cycle in SST is somewhat stronger in the Sargasso Sea than it is in the Nordic seas and (2) pCO_2 has a stronger dependence on SST in the Sargasso Sea. As shown in Fig. 5b there is good agreement between the predictions on ΔC_{eq}^{SST} from the MIT biogeochemical model and the results from the OWS stations.

3.5. Comparison with data

The predictions from the MIT biogeochemical model on C_T, NO_3 and total alkalinity A_T in the winter mixed layer (along the line defined in Fig. 1) are shown in Fig. 6. Starting with A_T, the relation seen in Fig. 6b reflects a prescribed relation between the total alkalinity concentration (normalized to 35 psu) and the temperature of the winter mixed layer. The predictions on the nitrate concentration are shown in Fig. 6c and agree fairly well with observations. However, the model gives slightly too low values overall, and this feature is especially pronounced at warm temperatures and in the 4–8 °C interval.

The predictions on C_T^W, along the transect defined in Fig. 1, are shown together with data in Fig. 6a. In the southernmost region, C_T^W is close to the dynamical equilibrium concentration. Otherwise, the MIT biogeochemical model predicts that the water has a rather constant undersaturation in the northern North Atlantic, although the C_T^W concentration increases monotonically towards north. The concentration increases northwards because of entrainment of carbon-rich deep water (and nutrient-rich water as seen in Fig. 6c) and the air–sea flux of CO_2.

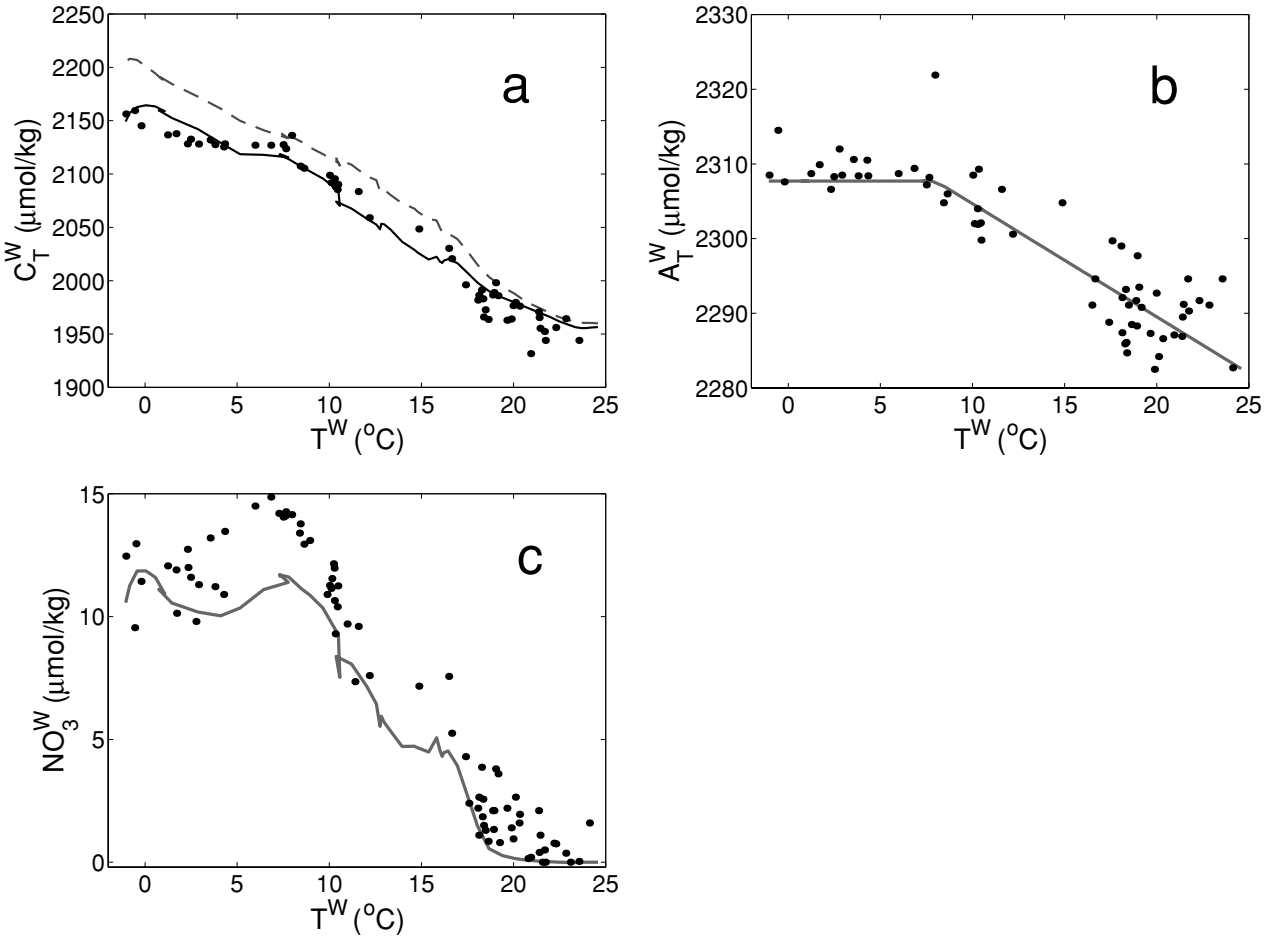

Fig 6. The predictions of the MIT biogeochemical along the transect in Fig. 1. The figure shows the modeled winter mixed layer concentrations of (a) the total dissolved inorganic carbon concentration, normalized to 35 psu (solid line) and the dynamical equilibrium concentration for the model (dashed line); (b) the total alkalinity concentrations, normalized to 35 psu, (full line); and (c) nitrate concentration (full line). Data (shown as dots) are extracted from the TTO/NAS expedition (Brewer et al. 1986) and represent the mean of the measurements between 80–200 m, which captures the remains of the winter mixed layer (Glover and Brewer, 1988).

The general picture is that the MIT biogeochemical model produces results that are in good agreement with the data. However, to generate such model results the alkalinity field, the nitrate field and the annual cycles in SST and biological production need to match the observations. The heat flux, or change in temperature, is one of the main drivers of the carbon cycle in the northern North Atlantic; thus, if the heat fluxes are wrong, the modeled carbon cycle will behave somewhat incorrectly as compared to nature. This can be seen in the model results for $C_{\mathrm{T}}^{\mathrm{W}}$ displayed in Fig. 6a: too strong heat fluxes in the temperature region 15–10 °C, imply that the system appears to be further away from equilibrium than is suggested by data. At lower temperatures, the heat flux is too weak, and the system is slightly too close to the dynamical equilibrium concentration.

4. A simple model for the "Gulf Stream" part of the North Atlantic

4.1. Outline of the simple model

The basic features of the oceanic carbon system can be illustrated using the simple model for $C_{\mathrm{T}}^{\mathrm{W}}$ presented in Section 2. Recapitulating eq. (10)

$$\frac{\partial}{\partial T^{\mathrm{W}}}\left(C_{\mathrm{T}}^{\mathrm{W}} - \gamma_{\mathrm{C:N}}\mathrm{NO}_3^{\mathrm{W}}\right) = \frac{\overline{F_{C_{\mathrm{T}}}}}{\overline{F_{\mathrm{T}}}},$$

where $\overline{F_{C_{\mathrm{T}}}}$ is given by eqs. (1) and (2). The first term reflects how $C_{\mathrm{T}}^{\mathrm{W}}$ changes with temperature; the second term is a diagnostic estimate of the net entrainment of carbon-rich deep water; and

the last term is the relative strength of the air–sea flux of CO_2 as compared to the heat flux.

The air–sea flux of CO_2 has a strong annual cycle; however, this cycle is included in the formulation $\overline{F_{C_T}} = \alpha(C_T^W - (C_{eq}^W + \Delta C_{eq}^{SST} + \Delta C_{eq}^B))$ presented in eqs. (1) and (2). The following parametrizations (which capture the main features of the predictions in Fig. 5) will be used:

$$\alpha = 1.2[160 - 4(T^W + 2)],$$
$$C_{eq}^W = f(T^W, S^W, pCO_2^A, A_T^W),$$
$$\Delta C_{eq}^{SST} = -(T^W + 2),$$
$$\Delta C_{eq}^B = 2.5NO_3^W(T^W). \quad (11a–d)$$

The factor of 1.2 is a correction on α that appears from the use of a continuous development of C_T^W in the model, whereas the parameters were estimated from a case with constant C_T^W (see the Appendix B). The function f determines the relation between the equilibrium of the total dissolved inorganic carbonate concentration and the following factors: the temperature, T^W; the salinity in the winter mixed layer, S^W; the atmospheric partial pressure of CO_2, $pCO^A{}_2$; and the total alkalinity, A_T^W (Peng et al. 1987). Here $pCO^A{}_2 = 340$ ppm, which is valid for 1981, or $pCO^A{}_2 = 360$ ppm which is valid for 1995. A_T^W is given by the piecewise linear function shown in (Fig. 6b) and NO_3^W is described by two linear functions that meet at $T^W = 8$ °C and are fitted towards data.

The heat loss $\overline{F_T}$ is given by

$$\overline{F_T} = H^W\left(Q_0 e^{-\beta T^W} + Q_1\right), \quad (12)$$

where $H^W = 500$ m, $Q_0 = 2$ °C yr^{-1}, $\beta = 0.2$ °C^{-1} and $Q_1 = 0.75$°C yr^{-1}. For the Nordic seas (i.e. between 8 and −1.8 °C), this corresponds to a mean temperature decrease of about 1.8 °C yr^{-1} in agreement with heat flux estimates for the Nordic seas (Häkkinen and Cavalieri, 1989; Simonsen and Haugan, 1996).

4.2. Model results

To solve eqs. (10)–(12), it is necessary to apply one boundary condition. The prescribed "best-fitting" piecewise linear relation for the nitrate concentration in the winter mixed layer implies that the nitrate concentration is zero at $T^W = 21.85$ °C. Thus, the integration start at this temperature with an initial value $C_T^W = 1950$ μmol kg^{-1} (or $C_T^W = 1964$ μmol kg^{-1} in the experiment for 1995, which give the same undersaturation in both experiments). With this boundary condition, it is possible to solve eqs. (10)–(12), and the resulting diagnostic estimate on C_T^W is shown in Fig. 7a. The predictions on the partial pressure of CO_2 in the winter mixed layer for 1981 is displayed in Fig. 7b and for 1995 in Fig. 7c. The C_T^W predicted from this simple model can be viewed either as a purely diagnostic concentration, or as the concentration of a water column that travels northwards with the large-scale North Atlantic circulation, presented in the temperature space. The simple model describes the data very well, showing that a simple model is possible for the selected part of the North Atlantic. Furthermore, the results from the simple model are close to the results from the MIT biogeochemical model, suggesting that the two models have similar dynamics. The results from the simple model will primarily be discussed, but the discussion should be valid for the MIT biogeochemical model as well.

The measurements as well as the model results show that the total dissolved inorganic carbon concentration increases by about 200 μmol kg^{-1} from the Sargasso Sea to the Nordic seas. Of this change, about 100 μmol kg^{-1} comes from entrainment of nutrient-rich deep water, and about 100 μmol kg^{-1} comes from the air–sea flux of CO_2. According to the model, the water column receives atmospheric CO_2 corresponding to 45 μmol kg^{-1} in the North Atlantic and 55 μmol kg^{-1} in the Nordic seas.

The air–sea flux of CO_2 is the result from changes in the dynamical equilibrium concentration between the southern and the northern North Atlantic, which is about 250 μmol kg^{-1}. The total contribution of the annual cycles in temperature and biological production on the dynamical equilibrium concentration is about 50 μmol kg^{-1}, or one-fifth of the total signal, which is a significant part of the total change. Accordingly, the annual cycles in sea surface temperature and biological production must be accounted for in a comprehensive study of the carbon cycle in the North Atlantic.

The analysis shows that the system is always undersaturated when the full annual cycle is considered, although the winter water may be oversaturated (cf. Figs. 7a and b). For temperatures between 7 and 10 °C there is a strong upwelling/entrainment of nutrients and carbon-rich deep water, which creates a system that is close to the equilibrium concentration. The closeness to the equilibrium concentration above 8 °C in the simple model is because of weak heat fluxes and large entrainment of NO_3 and C_T at these temperatures (Fig. 7a). The heat fluxes are higher in the MIT model, which creates a system that is further away from the equilibrium concentration (see Figs. 6a and 7a). Below 8 °C, the heat fluxes are larger and there is a net export of carbon from the upper ocean, this creates a system that is largely undersaturated in CO_2.

An important model parameter is the rate of change of the winter mixed-layer temperature, or the air–sea heat flux if mixing from deeper layers is neglected. Different water columns may take different pathways in the northward transport and experience different heat fluxes. The different $F_T(T^W)$ functions shown in Fig. 8 are therefore studied with the model. Case 2 refers to the standard case of eq. (12); case 1 refers to the situation where water is quickly brought up to the northern Nordic seas with an enhanced air–sea heat flux as the result; if the water stays in the more southern part of the Nordic seas, it will experience lower heat fluxes, and this is case 3. The model results from these different $F_T(T^W)$ functions are presented in Figs. 9a and b.

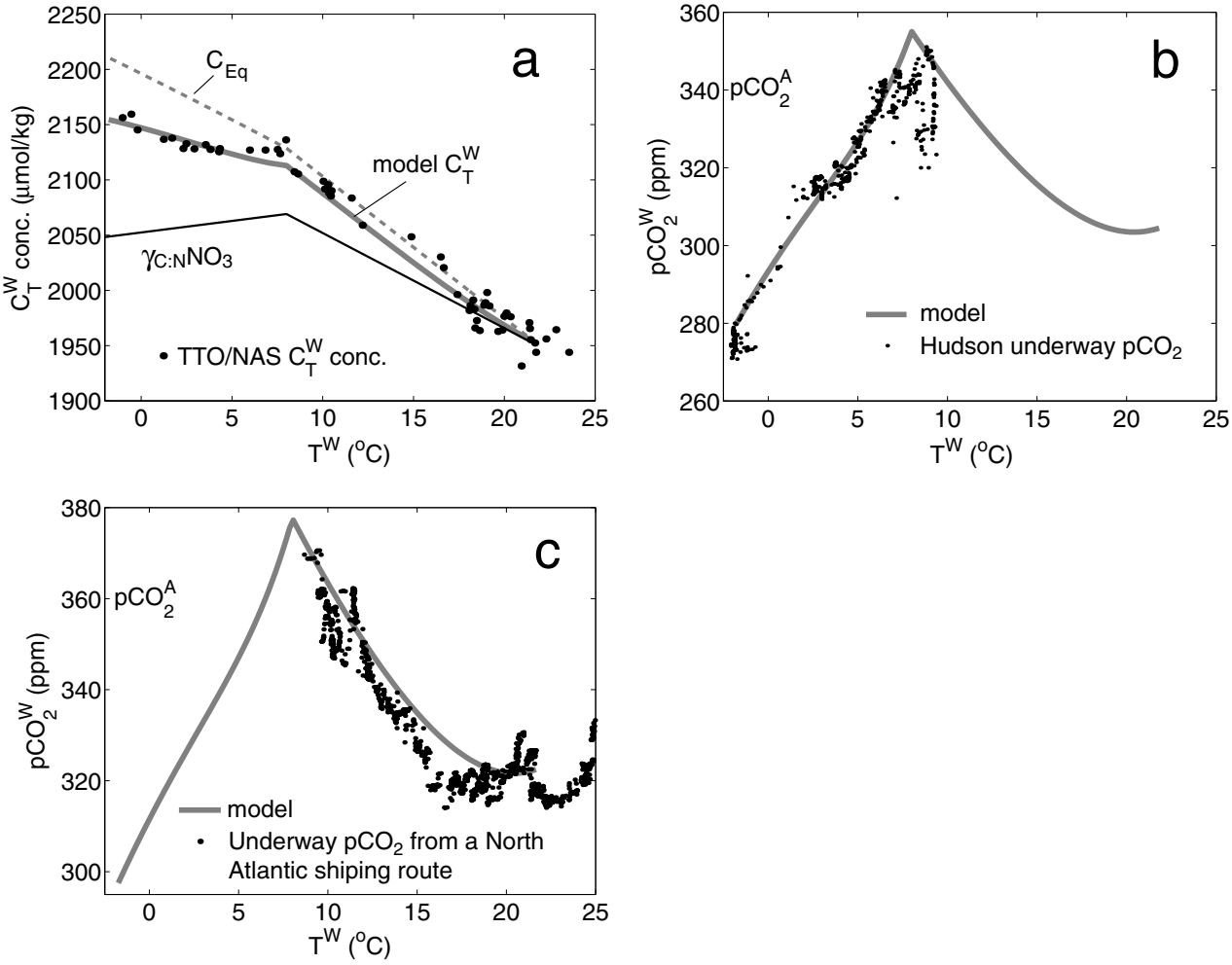

Fig 7. The predictions from the simple model for the North Atlantic. (a) The modeled C_T^W (normalized to 35 psu) in the winter mixed layer; data on C_T^W are extracted from the TTO/NAS data (Brewer et al. 1986). The entrainment of C_T from the deep water is diagnosed from a function that is fitted to the observed nitrate concentration in Fig. 3c. The effect from entrainment is shown as $\gamma_{C:N}$ NO_3 in the figure and represent the concentration that C_T^W would reach in the absence of air–sea flux of CO_2. (b) The model predictions on pCO_2 for the winter mixed layer; data are from the Hudson cruise in 1982, Leg 2 (Weiss et al. 1992). The atmospheric pCO_2 in this experiment is constant with value 340 ppm as indicated in the figure. (c) The model predictions on pCO_2 for the winter mixed layer for 1995; data are from a shipping route in the North Atlantic (Cooper et al. 1998). The atmospheric pCO_2 in this experiment is constant with value 360 ppm as indicated in (c).

From the results in Fig. 9a, it seems as if the different heat flux formulations have a small influence on the model with 30 μmol kg^{-1} C_T^W difference between cases 1 and 3. However, the uptake of atmospheric CO_2 in the Nordic seas is reduced by about 50% from case 3 to case 1. The sensitivity to the heat flux formulation is probably best seen in the modeled pCO_2^W, shown in Fig. 9b. Obviously, the uptake of CO_2 from the air is sensitive to the pathway of the water column. Thus, the description with a well-defined heat flux may be questioned. In reality, there will be an infinite number of water masses taking different pathways in $F_T(T^W)$ while subject to continuous mixing. To fully describe these features, it is probably necessary to find a more generalized description of the flows in temperature space, or the mass transport through isothermals in the upper ocean (cf. Walin, 1977; Speer et al. 1995; Marshall et al. 1999), and its coupling to the carbon cycle.

5. Discussion

The practice of mapping oceanic carbon system quantities to the temperature in order to extrapolate sparse measurements to a wider context is common. However, many of these studies do not provide a direct physical explanation for the relations used in the mapping procedure thereby introducing uncertainties in the method. In this study, a simple way to describe—and diagnose—the large-scale features of the oceanic carbon system is presented.

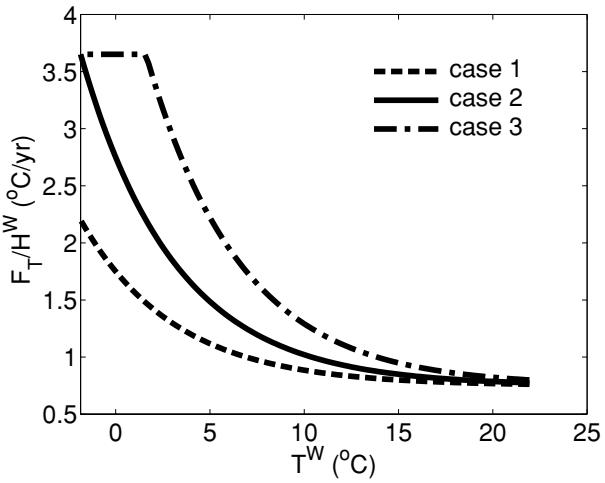

Fig 8. The three different heat fluxes used in the sensitivity study of the simple North Atlantic model.

The model focuses on the air–sea flux of CO_2 and the state that is in equilibrium with the atmosphere. The rate at which the system is able to approach equilibrium is slow for the carbon system; thus, the fact that there is a strong annual cycle in the oceanic pCO_2 implies that the state with zero annual flux will have substantial fluxes during the different seasons. In northern areas, which are dominated by strong cycles in new production, the state with zero annual flux is characterized by a seaward flux of CO_2 in summer and a flux of CO_2 toward the atmosphere in winter. The temperature cycle dominates over the production cycle in the southern areas and the state with zero annual flux will have seaward CO_2 fluxes in winter and a flux to the atmosphere in summer. The state that is in equilibrium with the atmosphere is thus a dynamical state where the air–sea fluxes change with season, but where these fluxes cancel out each other.

It is necessary to account for the annual cycles when estimating the dynamical equilibrium concentration and the rate of the equilibration process. It is not straightforward to carry out these calculations from the basic properties of the system (Broström, 2000). However, it may be shown that the air–sea flux of CO_2 can be described by $\overline{F_{C_T}} = \alpha(C_T^W - C_{eq})$. This simple formula, which captures the annual flux of CO_2, focuses on the slowly varying properties of the winter mixed layer, and enables a simple description of the system for time scales longer than one yr. However, to obtain a useful formulation, the impact of the annual cycles (e.g. of the sea surface temperature and biological production) must be given careful attention. An analysis of the impact of the annual cycles on the dynamical equilibrium concentration shows that ΔC_{eq}^B ranges between approximately 0 μmol kg^{-1} in the nutrient-depleted Sargasso Sea to about 20–30 μmol kg^{-1} in the Nordic seas. The impact of the SST cycle, ΔC_{eq}^{SST}, ranges between -25 μmol kg^{-1} in the Sargasso Sea to -5 μmol kg^{-1} in the Nordic seas. Thus, model studies of the oceanic carbon system that neglect the annual cycles (e.g. Sarmiento et al. 1995; Murnane et al. 1999) probably show too weak equator-to-pole forcing on the oceanic carbon cycle.

The air–sea flux of CO_2 is an important factor for the equilibration of the surface water; however, the model analysis shows that entrainment of carbon-rich deep water is an important factor as well. A water column that travels with the main north Atlantic circulation, starting at the Sargasso Sea and moving up to the Nordic seas, will lose heat and gain carbon by entrainment from deep water and from air–sea flux of CO_2. The models predict that the carbon concentration will be approximately 200 μmol kg^{-1} higher in the Nordic seas compared with the Sargasso Sea. Of this increase, about 100 μmol kg^{-1} is due to entrainment of carbon-rich deep water, and 100 μmol kg^{-1} comes from the air–sea flux of CO_2. Thus, both these processes must be described correctly.

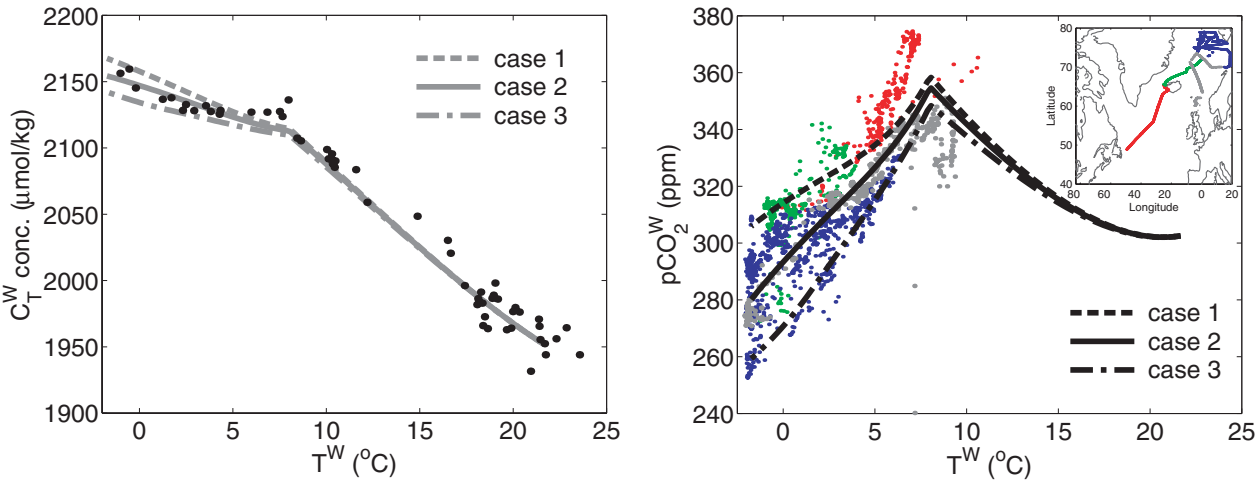

Fig 9. Model results for the three heat flux formulations displayed in Fig. 8. (a) the C_T^W concentration and (b) the partial pressure of CO_2 in the winter mixed layer. Data on pCO_2 are from the Hudson cruise in 1982 (Weiss et al. 1992) and the locations of the data are indicated by a color-coding.

The derived relationship between carbon-related variables and the temperature may also present a useful way to map the carbon system onto the temperature for the North Atlantic. Furthermore, the simplicity of the model may enable relatively simple assimilation of the carbon system variables using adjoint schemes (Ikeda and Sasai, 2000). However, to obtain the air–sea flux of CO_2 from the obtained fields, some model of the annual flux of CO_2 based on the winter values of the carbon system must also be presented (Broström, 2000).

6. Acknowledgments

I would like to thank Dr Mick Follows for helping me with the MIT biogeochemical ocean model, and Professor Gösta Walin for stimulating discussions on how the carbon cycle may be formulated. I am also grateful to the Knut and Alice Wallenberg foundation which sponsored a postdoctoral fellowship to MIT and computational resources.

7. Appendix A

The purpose of this appendix is to outline the approximations involved in rewriting

$$\frac{dQ_C}{d\xi} \approx \frac{dQ_T}{d\xi}\frac{dC}{dT}, \tag{A1}$$

where Q_C is the horizontal flux of a concentration C, Q_T is the horizontal flux of the temperature T and ξ is a coordinate along the flow. Notably, the flows are defined as being integrated over the depth of the winter mixed layer, H. The horizontal fluxes are given by advection and diffusion processes, thus

$$Q_C = HuC - H\kappa\frac{dC}{d\xi}, \tag{A2}$$

where u is the mean velocity over the winter mixed layer and κ is the horizontal diffusion coefficient. For clarity, lets consider the advection and diffusive parts separately; for advection

$$\left.\frac{dQ_C}{d\xi}\right|_{\text{advection}} = \frac{d}{d\xi}(HuC), \tag{A3}$$

which may be written as

$$\left.\frac{dQ_C}{d\xi}\right|_{\text{advection}} = Hu\frac{dC}{d\xi} + C\frac{d(Hu)}{d\xi}. \tag{A4}$$

Here it may be noted that if there is no mass flux through the bottom of the main thermocline it would follow from mass conservation that $u \sim H^{-1}$; in this case the last term is identically zero. Figure A1, which displays the annual mean value of $|uH|$, shows that $|uH|$ do not vary significantly along the northward drift in the North Atlantic despite the fact that horizontal advection in the thermocline is important for the subduction rate in the North Atlantic (Marshall et al. 1993). Therefore it seems reasonable to neglect the last term in eq. (A4).

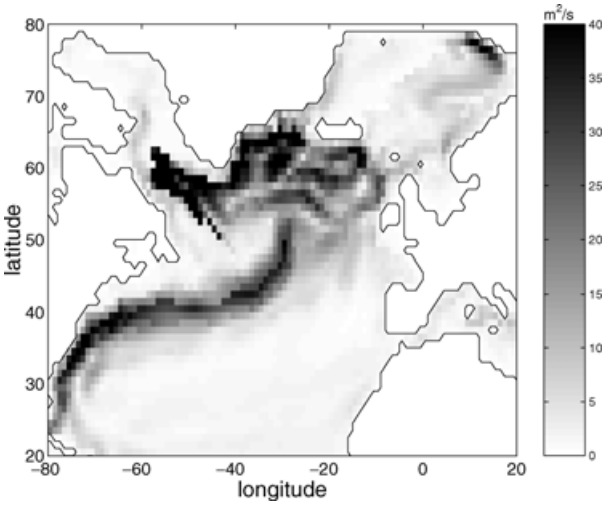

Fig A1. The annual mean of $-\int_{-H}^{0}\sqrt{u^2+u^2}dz$ in the North Atlantic. Here, H is the depth of the winter mixed layer and is defined as the depth where the temperature deviates more than 0.2 °C from the surface water in February, and u, v are the horizontal velocities in the model.

Neglecting the last term in eq. (A4)

$$\left.\frac{dQ_C}{d\xi}\right|_{\text{advection}} \approx Hu\frac{dC}{d\xi} \tag{A5}$$

and a straightforward application of the chain rule for derivatives gives

$$\left.\frac{dQ_C}{d\xi}\right|_{\text{advection}} \approx Hu\frac{dT}{d\xi}\frac{dC}{dT}. \tag{A6}$$

Applying eq. (A5) to temperature

$$\left.\frac{dQ_T}{d\xi}\right|_{\text{advection}} \approx Hu\frac{dT}{d\xi}. \tag{A7}$$

Combining eqs. (A6) and (A7) gives

$$\left.\frac{dQ_C}{d\xi}\right|_{\text{advection}} \approx \left.\frac{dQ_T}{d\xi}\right|_{\text{advection}}\frac{dC}{dT}. \tag{A8}$$

showing that eq. (A1) is approximately valid for the advection component of the system.

The diffusive fluxes are generally smaller than the advective fluxes and could in principle be neglected altogether. However, it may be interesting to see what approximations are needed for eq. (A1) to be true for the diffusive fluxes as well.

For the diffusive flux

$$\left.\frac{dQ_C}{d\xi}\right|_{\text{diffusion}} = -\frac{d}{d\xi}\left[H\kappa\frac{dC}{d\xi}\right], \tag{A9}$$

or

$$\left.\frac{dQ_C}{d\xi}\right|_{\text{diffusion}} = -\frac{d(H\kappa)}{d\xi}\frac{dC}{d\xi} - H\kappa\frac{d}{d\xi}\frac{dC}{d\xi}; \tag{A10}$$

applying the chain rule

$$\left.\frac{dQ_C}{d\xi}\right|_{\text{diffusion}} = -\frac{d(H\kappa)}{d\xi}\frac{dC}{d\xi} - H\kappa\frac{d}{d\xi}\left(\frac{dT}{d\xi}\frac{dC}{dT}\right), \tag{A11}$$

which is readily written as

$$\left.\frac{dQ_C}{d\xi}\right|_{\text{diffusion}} - \frac{d(H\kappa)}{d\xi}\frac{dC}{d\xi} - H\kappa\frac{d^2T}{d\xi^2}\frac{dC}{dT} - H\kappa\frac{dT}{d\xi}\frac{d^2C}{d\xi dT}. \tag{A12}$$

Figure 6a shows that C_T varies almost linearly with temperature in the winter mixed layer. Accordingly, $dC_T/dT \approx$ constant, which implies that its derivative with respect to ξ is approximately zero, and the last term in eq. (A13) may be ignored

$$\left.\frac{dQ_C}{d\xi}\right|_{\text{diffusion}} \approx -\frac{d(H\kappa)}{d\xi}\frac{dC}{d\xi} - H\kappa\frac{d^2T}{d\xi^2}\frac{dC}{dT}. \tag{A13}$$

Using the chain rule for derivatives

$$\left.\frac{dQ_C}{d\xi}\right|_{\text{diffusion}} \approx -\left[\frac{d(H\kappa)}{d\xi}\frac{dT}{d\xi} + H\kappa\frac{d^2T}{d\xi^2}\right]\frac{dC}{dT}, \tag{A14}$$

or by applying eq. (A10)

$$\left.\frac{dQ_C}{d\xi}\right|_{\text{diffusion}} \approx \left.\frac{dQ_T}{d\xi}\right|_{\text{diffusion}}\frac{dC}{dT}. \tag{A15}$$

Showing that

$$\frac{dQ_C}{d\xi} \approx \frac{dQ_T}{d\xi}\frac{dC}{dT}, \tag{A16}$$

within the approximations outlined in this Appendix.

8. Appendix B

In eq. (1) and the results shown in Fig. 5a, α is defined and calculated for one yr of integration where C_T^W represent a constant value. Thus, if C_T^W increases monotonously in the model, the air–sea flux of CO_2 calculated according to the formula $\overline{F_{C_T}} = \alpha(C_T^W - C_{eq})$ becomes too small. To compensate for this non-physical situation, the value of α is increased to α' in the model.

If the annual flux, where C_T^W changes with time, should be the same as in the case where C_T^W is constant, the following formula applies:

$$\int_o^T \alpha(C_T^W(t_0) - C_{eq})dt = \int_o^T \alpha'\left(C_T^W(t) - C_{eq}\right)dt, \tag{B1}$$

where $T = 1$ yr and $C_T^W(t_0)$ is the concentration at the start of the integration. The interest here is on the strength of air–sea gas exchange, and the physical mixing and the export by organic particles are neglected in this calculation. Thus, the time evolution of C_T^W in a column with depth H^W becomes

$$H^W\frac{dC_T^W(t)}{dt} = -\alpha'\left(C_T^W(t) - C_{eq}\right), \tag{B2}$$

where H^W is the depth of the winter mixed layer. By solving Eqs. (B1) and (B2) it follows that $\alpha' \sim 1.2\alpha$ if $H^W = 500$ m.

References

Brewer, P. G., Takahashi, T. and William's, R. T. 1986. Transient tracers in the ocean (TTO)–hydrographic data and carbon dioxide systems with revised carbon chemistry data. NDP-004/R1, Carbon Dioxide Information Analysis Center (CDIAC), Oak Ridge National Laboratory, Oak Ridge, TN.

Broecker, W. S. and Peng, T.-H. 1982. Tracers in the sea. Eldigo Press, Lamont-Doherty Geological Observatory, Palisades, NY, 690 pp.

Broecker, W. S., Takahashi, T. and Peng, T.-H. 1985. Reconstruction of past atmospheric CO_2 contents from the chemistry of the contemporary ocean: an evaluation. DOE/OR.857, DOE Technical Report.

Broström, G. 1997. Air–sea flux of CO_2—can we short cut the annual cycle? A Norwegian Sea case study. *Phys. Chem. Earth* **21**, 517–522.

Broström, G. 1998. A note on the C/N and C/P ratio of the biological production in the Nordic Seas. *Tellus* **50B**, 93–109.

Broström, G. 2000. The role of the seasonal cycles for the air–sea exchange of CO_2. *Mar. Chem.* **72**, 151–169.

Chen, C.-T. A., Jones, E. P. and Lin, K. 1990. Wintertime total carbon dioxide measurements in the Norwegian and Greenland seas. *Deep-Sea Res.* **37**, 1455–1473.

Cooper, D. J., Watson, A. J. and Ling, R. D. 1998. Variations of pCO_2 along a North Atlantic shipping route (UK to Jamaica): a year of automated observations. *Mar. Chem.* **60**, 147–164.

Daly, K. L., Wallace, D. W. R., Smith, W. O., Skoog, A., Lara, R. and coauthors. 1999. Non-Redfield carbon and nitrogen cycling in the Arctic: effects of ecosystem structure and dynamics. *J. Geophys. Res.* **104**, 3185–3199.

Feely, R. A., Wanninkhof, R., Takahashi, T. and Tans, P. 1999. Influence of El Niño on the equatorial Pacific contribution to atmospheric CO_2 accumulation. *Nature* **398**, 597–601.

Follows, M. J., Williams, R. G. and Marshall, J. C. 1996. The solubility pump of carbon in the subtropical gyre of the North Atlantic. *J. Mar. Res.* **54**, 605–630.

Gent, P. R., Willebrand, J., McDougall, T. J. and McWilliams, J. C. 1995. Parameterizing eddy-induced tracer transports in ocean circulation models. *J. Phys. Ocean.* **25**, 463–474.

Glover, D. M. and Brewer, P. G. 1988. Estimates of wintertime mixed layer nutrient concentrations in the North Atlantic. *Deep-Sea Res.* **35**, 1525–1546.

Häkkinen, S. and Cavalieri, D. J. 1989. A study of oceanic surface heat fluxes in the Greenland, Norwegian, and Barents seas. *J. Geophys. Res.* **94**, 6145–6157.

Ikeda, M. and Sasai, Y. 2000. Reconstruction of subsurface DIC and alkalinity fields in the North Pacific using assimilation of upper ocean data. *Mar. Chem.* **72**, 343–358.

Körtzinger, A., Koeve, W., Kähler, P. and Mintrop, L. 2001. C:N ratios in the mixed layer during the productive season in the northeast Atlantic Ocean. *Deep-Sea Res.* **48**, 661–688.

Lee, K., Wanninkhof, R., Takahashi, T., Doney, S. C. and Feely, R. A. 1998. Low interannual variability in recent oceanic uptake of atmospheric carbon dioxide. *Nature* **396**, 155–159.

Lefèvere, N. and Taylor, A. 2002. Estimating pCO_2 from sea surface temperatures in the Atlantic gyres. *Deep-Sea Res.* **49**, 539–554.

Loukos, H., Vivier, F., Murphy, P. and Harrison, D. E. 2000. Variability of the carbon dioxide evasion rates in the equatorial Pacific from 1982 to 1993 estimated from monthly temperature and salinity data. *Geophys. Res. Lett.* **27**, 1735–1738.

Marshall, J., Adcroft, A., Hill, C., Perelman, L. and Heisey, C. 1997a. A finite-volume, incompressible Navier Stokes model for studies of the ocean on parallel computers. *J. Geophys. Res.* **102**, 5753–5766.

Marshall, J., Hill, C., Perelman, L. and Adcroft, A. 1997b. Hydrostatic, quasi-hydrostatic, and nonhydrostatic ocean modeling. *J. Geophys. Res.* **102**, 5733–5752.

Marshall, J., Jamous, D. and Nilsson, J. 1999. Reconciling thermodynamic and dynamic methods of computation of water-mass transformation rates. *Deep-Sea Res.* **46**, 545–572.

Marshall, J. C., Nurser, A. J. G. and Williams, R. G. 1993. Inferring the subduction rate and period over the North Atlantic. *J. Phys. Ocean.* **23**(7), 1315–1329.

Murnane, R. J., Sarmiento, J. L. and Le Quèrè, C. 1999. Spatial distribution of air–sea CO_2 fluxes and the interhemispheric transport of carbon by the oceans. *Global Biogeochem. Cycles* **13**, 287–305.

Peng, T.-H., Takahashi, T., Broecker, W. S. and Olafsson, J. 1987. Seasonal variability of carbon dioxide, nutrients and oxygen in the northern North Atlantic surface water: observations and a model. *Tellus* **39B**, 439–458.

Sabine, C. L. and Key, R. M. 1998. Controls on fCO_2 in the South Pacific. *Mar. Chem.* **60**, 95–110.

Sambrotto, R. N., Savidge, G., Robinson, C., Boyd, P., Takahashi, T. and coauthors. 1993. Elevated consumption of carbon relative to nitrogen in the surface ocean. *Nature* **363**, 248–250.

Sarmiento, J. L., Murnane, R. and Le Quèrè, C. 1995. Air–sea CO_2 transfer and the carbon budget of the North Atlantic. *Phil. Trans. R. Soc. Lond. B.* **384**, 211–219.

Simonsen, K. and Haugan, P. M. 1996. Heat budgets of the Arctic, Mediterranean and sea surface heat flux parametrizations for the Nordic seas. *J. Geophys. Res.* **101**, 6553–6576.

Speer, K. G., Isemer, H. J. and Biastoch, A. 1995. Water mass formation from revised COADS data. *J. Phys. Ocean.* **25**, 2444–2457.

Stephens, M. P., Samuels, G., Olson, D. B. and Fine, R. A. 1995. Sea-air flux of CO_2 in the North Pacific using shipboard and satellite data. *J. Geophys. Res.* **100**, 13 571–13 583.

Takahashi, T., Olafsson, J., Goddard, J. G., Chipman, D. W. and Sutherland, S. C. 1993. Seasonal variation of CO_2 and nutrients in the high latitude surface oceans: A comparative study. *Global Biogeochem. Cycles* **7**, 843–878.

Tans, P. P., Fung, I. and Takahashi, T. 1990. Observational constraints on the global atmospheric CO_2 budget. *Science* **247**, 1431–1438.

Walin, G. 1977. A theoretical framework for the description of estuaries. *Tellus* **29**, 128–136.

Watson, A. J., Robinson, C., Robertson, J. E., Williams, P. J. leB. and Fasham, M. J. R. 1991. Spatial variability in the sink for atmospheric carbon dioxide in the North Atlantic. *Nature* **350**, 50–53.

Weiss, R., von Woy, F. and Salameh, P. K. 1992. Surface water and atmospheric carbon dioxide and nitrous oxide observations by shipboard automated gas chromatography: results from expeditions between 1977 and 1990., Scripps Institution for Oceanography. Reference 92-11. ORNL/CDIAC-59, Carbon Dioxide Information Analysis Centre, Oak Ridge National Laboratory, Oak Ridge, TN.